

Deregulated matriptase activity in oral squamous cell carcinoma promotes the infiltration of cancer-associated fibroblasts by paracrine activation of protease-activated receptor 2

Ai Kanemaru,¹ Koji Yamamoto,¹ Makiko Kawaguchi,¹ Tsuyoshi Fukushima,¹
Chen-Yong Lin,² Michael D. Johnson,² Eric Camerer,³ and Hiroaki Kataoka^{1*}

¹Section of Oncopathology and Regenerative Biology, Department of Pathology,
Faculty of Medicine, University of Miyazaki, Miyazaki, Japan

²Lambardi Comprehensive Cancer Centre, Georgetown University, School of Medicine,
Washington, DC, USA;

³INSERM U970, Paris Cardiovascular Research Centre, Paris, France.

Correspondence: Hiroaki Kataoka, Section of Oncopathology and Regenerative Biology,
Department of Pathology, Faculty of Medicine, University of Miyazaki, 5200 Kihara,
Kiyotake, Miyazaki, Japan. Tel: +81-985-852809; Fax: +81-985-856003; E-mail:
mejina@med.miyazaki-u.ac.jp

Short title: Matriptase augments CAF recruitment

Key words: oral squamous cell carcinoma, cancer-associated fibroblasts, matriptase,
protease-activated receptor 2, HAI-1

Abbreviations: CAF: cancer-associated fibroblasts; HAI: hepatocyte growth factor activator inhibitor; OSCC: oral squamous cell carcinoma; SFCM: serum-free conditioned medium; PAR: protease-activated receptor (PAR); HGF: hepatocyte growth factor; TTSP: type II transmembrane serine protease; PDGF: platelet-derived growth factor; TGF: transforming growth factor; bFGF: basic fibroblast growth factor; SMA: α -smooth muscle actin; pAb: polyclonal antibody; mAb: monoclonal antibody; DMEM: Dulbecco's modified Eagle's medium; FBS: fetal bovine serum; PBS: phosphate buffered saline; GAPDH: glyceraldehyde 3-phosphate dehydrogenase; TBS: Tris buffered saline; OS: overall survival; DFS: disease-free survival

Research article category: Tumor Immunology and Microenvironment

Brief description

Cancer-associated fibroblasts (CAFs) contribute to cancer progression. This study provides evidence for the first time that cancer cell-derived matriptase induces migration of CAFs in oral squamous cell carcinomas (OSCC) through paracrine activation of protease-activated receptor 2 (PAR-2) expressed by CAFs.

Immunohistochemical analysis of resected OSCC tissues revealed that 35% of cases showed PAR-2 immunoreactivity in CAFs, and this tended to correlate with more invasive histology and shorter disease-free survival.

ABSTRACT

Cancer-associated fibroblasts (CAFs) are known to contribute to cancer progression. We have reported that cell surface expression of hepatocyte growth factor activator inhibitor 1 (HAI-1) is decreased in invasive oral squamous cell carcinoma (OSCC) cells. This study examined if HAI-1-insufficiency contributes to CAF recruitment in OSCC. Serum-free conditioned medium (SFCM) from a human OSCC line (SAS) stimulated the migration of 3 human fibroblast cell lines, NB1RGB, MRC5 and KD. SFCM from HAI-1-knockdown SAS showed an additive effect on the migration of NB1RGB and MRC5, but not KD. SAS SFCM induced protease-activated receptor-2 (PAR-2) expression in NB1RGB and MRC5, but not in KD, and a PAR-2 antagonist blocked the stimulatory effect of HAI-1 knockdown on migration of the PAR-2 expressing cell lines. Moreover, HAI-1-deficient SFCM showed additive stimulatory effects on the migration of wild-type but not PAR-2-deficient mouse fibroblasts. Therefore, the enhanced migration induced by HAI-1-insufficiency was mediated by PAR-2 activation in fibroblasts. This activation resulted from the deregulation of the activity of matriptase, a PAR-2 agonist protease. HAI-1 may thus prevent CAF recruitment to OSCC by controlling matriptase activity. When HAI-1 expression is reduced on OSCC, matriptase may contribute to CAF accumulation by paracrine activation of fibroblast PAR-2. Immunohistochemical analysis of resected OSCC revealed increased PAR2-positive CAFs in 35% (33/95) of the cases studied. The increased PAR-2 positive CAFs tended to correlate with infiltrative histology of the invasion front and shorter disease-free survival of the patients.

Introduction

Oral squamous cell carcinoma (OSCC) is the most common cancer of the head and neck, and sixth most common cancer worldwide (1). Despite recent advances in treatment protocols, the long-term survival of OSCC patients has remained at 50-60% (2). The high mortality from OSCC is attributed to a high degree of local invasiveness, and regional and distant metastases (2). Therefore, a more detailed analysis of the molecular mechanisms underlying invasive growth of OSCC is required for the development of novel treatment strategies. Cooperation between cancer cells and stromal cells in the tumor microenvironment is essential for malignant progression of solid cancer. This important area of cancer research has become a potential target for therapeutic intervention (3). Extracellular proteolysis has significant roles in the tumor microenvironment through remodeling of extracellular matrices, processing of pericellular growth factors, and activation of cell surface protease-activated receptors (PARs) (3-6). Therefore, regulation of pericellular protease activity may have therapeutic implications in the progression of cancers, including OSCC.

Hepatocyte growth factor activator inhibitors (HAI) constitute a family of type I transmembrane Kunitz-type serine protease inhibitors, initially identified as potent inhibitors of hepatocyte growth factor (HGF) activator, which is a serum protease that efficiently activates pro-HGF (7). Two family members have been reported, namely HAI-1 and HAI-2, both of which have two extracellular Kunitz-type serine protease inhibitor domains (8, 9). Subsequent studies revealed that membrane-associated serine proteases with trypsin-like activity are primary targets of both HAIs (10). HAI-1 is expressed by most epithelial cells and placental trophoblasts (11-13), and its most important cognate protease on the epithelial cell surface is matrilysin, a type II

transmembrane serine protease (TTSP). Other TTSPs such as hepsin, human airway trypsin, and TMPRSS13, as well as a glycosylphosphatidylinositol-anchored serine protease prostasin, are also sensitive to HAI-1 (10, 14-17). In our previous study using human tumor tissues from surgically resected OSCC specimens, membrane-associated HAI-1 immunoreactivity of tumor cells was decreased in the invasion front and may be associated with an increased presence of cancer-associated fibroblasts (CAFs) (18). Therefore, we hypothesized that the loss of HAI-1 might have a causal role in the recruitment of CAFs. Some evidence suggests that insufficient HAI-1 activity enhances pericellular serine protease activities, particularly of matriptase (18-21). Matriptase is one of the most studied TTSPs and has important roles in carcinogenesis and cancer progression (10, 22, 23). It has a wide range of substrates and is responsible for the activation of pro-HGF, pro-urokinase, pro-prostasin, platelet-derived growth factor (PDGF)-D and PAR-2 (10, 23, 24).

PAR-2 is a seven transmembrane spanning domain G protein-coupled receptor that is activated by trypsin, coagulation factor VII/tissue factor complex, coagulation factor Xa, and tryptase (5). Recent evidence indicates that matriptase is also an important activator of PAR-2 (21, 23, 25, 26). The proteolytic activation of PAR-2 induces various cellular responses, including migratory activity (6). PAR-2 is predominantly expressed on epithelial, endothelial, and smooth muscle cells (6). Whereas normal fibroblasts hardly express any PAR-2, activated fibroblasts express PAR-2 in inflammatory conditions (27-30). PAR-2 expression can be induced in fibroblasts by the addition of PDGF, transforming growth factor (TGF)- β , or basic fibroblast growth factor (bFGF) (27, 28), all of which are observed in cancer tissues. Indeed, proliferating fibroblasts within the stroma immediately surrounding tumors

specifically expressed PAR-2 (31). Therefore, it is reasonable to postulate that increased matriptase activity in tumor tissue activates PAR-2 expressed on the cell surface of CAFs. In this study, we assessed the possible involvement of the activation of fibroblast PAR-2 in CAF recruitment at the invasion front of OSCC, where cell surface HAI-1 frequently decreases.

Materials and Methods

Antibodies

Anti-human HAI-1 goat polyclonal antibody (pAb) was purchased from R & D Systems (Minneapolis, MN, USA). Anti-human HAI-1 mouse monoclonal antibody (mAb) 1N7 and anti-human matriptase mouse mAb M24 were reported previously (11, 32). Anti-human matriptase sheep pAb and anti-active matriptase rabbit mAb (clone A11) was from R & D Systems and Millipore (Billerica, MA, USA) (33), respectively. Anti-PAR-2 mouse mAb SAM11 was from Santa Cruz Biotechnology (Santa Cruz, CA). The epitope of SAM11 is Ser37-Gly50 of human PAR-2 protein and it crossreacts to mouse PAR-2. Anti-human α -smooth muscle cell actin (SMA) mouse mAb was from Dako (Carpinteria, CA, USA), anti-caveolin 1 mouse mAb was from Cell Signaling Technology (Tokyo, Japan) and anti- β -actin mouse mAb was from Sigma (St Louis, MO, USA).

Cell culture and preparation of serum-free conditioned medium (SFCM)

The SAS cell line was obtained from the Cell Resource Center for Biomedical Research (Tohoku University, Sendai, Japan). The identity of the SAS cell line and its sublines used in this study was confirmed by short tandem repeat DNA profiles

(TAKARA BIO Inc., Shiga, Japan). Human fibroblast cell lines NB1RGB, MRC5 and KD were obtained from the Riken Cell Bank (Tsukuba, Japan), Japanese Cancer Research Resources Bank (Tokyo, Japan), and Japan Health Science Foundation, (Tokyo, Japan), respectively. NB1RGB, MRC5, and KD were established from human skin, lung, and lip, respectively. They were cultured in Dulbecco's modified Eagle's medium (DMEM) containing 10% fetal bovine serum (FBS). To obtain PAR-2-deficient murine fibroblasts, the dermal tissue was prepared from 1 day-old *F2r11^{-/-}* C57BL/6 mice (34). Littermate control fibroblasts were obtained from wild-type and *F2r11^{+/-}* C57BL/6 mice. For primary culture of dermal fibroblasts, the dermis was minced and incubated in DMEM containing collagenase type X (1 mg/mL; Wako, Osaka, Japan)/dispase (500 U/mL; GIBCO, Grand Island, NY., USA) at 37°C for 30 min. Dissociated cells were seeded onto 100-mm dishes and cultured in DMEM supplemented with 10% FBS. All animal experiments were approved by the Animal Care and Use Committee of the University of Miyazaki (Miyazaki, Japan).

The establishment of the SAS subline with stable silencing of the *Spint1* gene (HAI-1^{Low}) and SAS/HAI-1^{Low} with engineered reversion of HAI-1 (HAI-1^{High}) have been reported previously (18). Short-hairpin RNA (shRNA) expression retroviral vector pSINsi-hU6 (Takara Bio, Osaka, Japan) with the target sequence of the *Spint1* gene (5'-GGGCAGGCATAGACTTGAAGG) was used, and a stable G418 (Nacalai Tesque, Kyoto, Japan)-resistant cell pool was selected. For stable reversion of HAI-1 in HAI-1^{Low} cells, human HAI-1 cDNA was subcloned into pLenti6.3/TO/V5 (Life Technologies, Tokyo, Japan) Generation of the lentiviral particles and transfection were performed according to the manufacturer's instructions. Then, a blasticidin (Invitrogen, Carlsbad, CA, USA)-resistant HAI-1 reversion cell pool, HAI-1^{High} was obtained.

To obtain SFCM from SAS cells, cultured cells at 30 % confluency were washed three times with phosphate-buffered saline (PBS), followed by cultivation in serum-free DMEM. Forty-eight hours later, SFCM was collected and centrifuged at 1000 rpm for 5 minutes to remove insoluble cellular debris. SFCM was concentrated 10-fold by ultrafiltration using Amicon Ultra filter units (4 mL, 10 kDa cut-off) (Millipore), and the concentration of proteins in the concentrated SFCM was measured with the Bradford method (Bio-Rad, Hercules, CA, USA).

***In vitro* motility and proliferation assays**

In vitro cellular motility was evaluated using ThinCert™ (pore size 8 μm; Greiner Bio-One, Tokyo, Japan), as described (18). Cells (1×10^4 in 100 μL DMEM/0.1 % BSA) were placed in the upper compartment. The lower compartment contained serum-free DMEM/0.1% BSA mixed with SFCM equivalent to 2 μg of total protein or 5 nM of recombinant human matriptase catalytic domain (R & D systems). After incubation for 4 h, the cells that had migrated to the lower surface were stained with hematoxylin and counted in nine randomly selected $\times 400$ fields. To examine the role of PAR-2, cells were incubated in the presence or absence of 10 μM of FSLLRY-NH₂, a PAR-2 antagonist, (Peptide International, Louisville, KY, USA). Cell proliferation *in vitro* was assessed using the cell counting kit-8 (Wako). Cells were seeded in 96-well tissue culture plates (10,000 cells/well) in serum-free DMEM with or without SAS SFCM. After four days of culture, the relative cell number was assessed according to the manufacturer's instruction.

Reverse transcription-polymerase chain reaction (RT-PCR)

For analysis of PAR-2 expression levels in fibroblasts, cells were seeded in 24-well tissue culture plates. Cells were incubated for an additional 1 hour in serum-free DMEM with or without SAS SFCM. Total cellular RNA was extracted by Trizol (Invitrogen), and three μg of total RNA was reverse transcribed with a mixture of oligo dT and random primers (2.5 μM each) (Takara Bio) using ReverTraAce™ (TOYOBO, Osaka, Japan) according to the manufacturer's instruction. Resulting cDNA was subjected to PCR using the following amplification primers. Human *F2RL1* (PAR-2): 5'GAATCAGGTTTCCAATCAACAGCA3'(forward); 5'GGTACAAGAACCTCACTCACTGGAC3'(reverse). Human *ACTB* (β -actin): 5'ATTGCCGACAGGATGCAGA3'(forward); 5'GAGTACTTGCGCTCAGGAGGA3'(reverse). Mouse *F2r1l* (PAR-2): 5'ACCGGGACGCAACAACAGTAAAG3'(forward); 5'CCATGCCATTACTGGGCAAACC3' (reverse). Mouse *Gapdh* (glyceraldehyde 3-phosphate dehydrogenase: GAPDH): 5'GGTGAAGGTCGGTGTGAACG3'(forward); 5'GTGAAGACACCAGTAGACTC3'(reverse). Mouse *Adgre1* (F4/80): 5'CCTATCTGTGTCTCCTGGAAC3'(forward); 5'GTGCAGCATCTTGATGTTGCG3'(reverse).

Matriptase activity assay and knock down

To measure matriptase activity in SFCM, the fluorogenic substrate t-butyloxycarbonyl-[(2S)-2-amino-4-(benzyloxycarbonyl)butanoyl]-L-alanyl-L-arginine 4-methylcoumaryl-7-amide [Boc-Glu(OBzl)-Ala-Arg-AMC] (Peptide Institute, Osaka, Japan) was added to the medium (final concentration 10 μM) in a 96-well plate (Corning, NY, USA), and the generation of fluorescence was measured using

FlexStation 3 (Molecular Devices, Tokyo, Japan). The activity was expressed either by relative fluorescence unit (RFU) at each time point or the calculated maximum slope of the hydrolysis rate (velocity max: Vmax). For transient silencing of matriptase, two kinds of small interfering RNA (siRNA) were used as described previously (19, 21). One (mat siRNA #1) was Stealth™ siRNA (Invitrogen) and the sequence was 5'-GCGUGUACACAAGGCUCCUCUGUU-3'. Stealth siRNA Negative Control Duplexes (Invitrogen) were transfected as a control. Another siRNA sequence (mat siRNA#2) was 5'-CGUCGUCACUUGUACACCAdTdT-3'. In this case, scrambled siRNA was used as a control. Transfection was performed using Lipofectamine 2000 reagent (Invitrogen) followed by cultivation in DMEM supplemented with 10% FBS for 24 h.

Immunoblot analysis

For matriptase immunodetection, cell lysates were collected in 1 % TritonX-100, and protease inhibitor cocktail (1:40) (P8340; Sigma) in PBS. Cellular debris was removed by centrifugation (15,400 g for 15 min at 4°C). For detection of PAR-2, cells were washed with PBS once, followed by hypotonic treatment with distilled water for 30 sec. The swollen cells were mechanically resuspended in 5 mM Tris (pH 7.5) containing 0.5 mM EDTA and protease inhibitor cocktail. Cellular debris was removed by centrifugation (1000 g for 10 min at 4°C), and the supernatant was subjected to ultracentrifugation (99,000 g) for 1 h at 4°C. The pellet, containing a crude membrane fraction, was resuspended in 50 mM Tris (pH 7.5) with 150 mM NaCl (TBS), containing 5 mM EDTA, 1 % Triton X-100 (v/v) and proteinase inhibitor cocktail. Then the sample was separated by SDS-PAGE using a 10 % resolving layer and a 4 %

stacking layer and transferred to a PVDF membrane (Millipore). After blocking with 5 % skim milk in TBS with 0.05 % (v/v) Tween-20 (pH7.6) (TBS-T), the membrane was incubated overnight (4°C) with primary antibody. Following washing in TBS-T, membranes were incubated with peroxidase-conjugated goat anti-mouse IgG (Bio-Rad) for 1 h. The labeled proteins were visualized with a chemiluminescence reagent (PerkinElmer Japan, Yokohama, Japan).

Clinicopathological study cohort

The study protocol was in accordance with the revised Helsinki Declaration of 1983 and approved by the Institutional Review Board of the Faculty of Medicine, University of Miyazaki. The demographic characteristics of OSCC patients who were included in the analysis are summarized in Supplemental Table 1. A total of 95 Japanese patients were included in this study, and they did not receive adjuvant therapy prior to surgery. All patients underwent surgery at the University of Miyazaki Hospital between April 2000 and November 2011. The patients' ages ranged from 28- to 96-years-old, with mean and median ages of 68.4 and 69, respectively. The postoperative median follow-up period was 3.42 years (maximum 13.4 years), while the median disease-free interval was 2.17 years. During the follow-up period, 13 patients died of OSCC, and 4 patients died of other causes. Forty-five cases received neoadjuvant therapy after surgery. Overall survival (OS) and postoperative disease-free survival (DFS) were defined as the time from the date of surgery to the date of death and from the date of initial detection of local OSCC recurrence or distant OSCC metastasis, respectively. Histopathological classification of the OSCC invasion pattern was performed according to Bryne et al. as follows (35): grade 1, pushing,

well-delineated border; grade 2, infiltrating solid nests and/or strands; grade 3, small groups or cords of infiltrating cells; grade 4, marked and widespread cellular dissociation in small groups and/or single cells.

Immunohistochemical and immunofluorescence analyses

Immunohistochemistry was performed on formalin-fixed, paraffin-embedded tissue sections. Slides were stained for PAR-2 (SAM11, 1:250), HAI-1 (1N7, 10 µg/mL), and matriptase (sheep pAb, 1:200) using Envision-labeled polymer reagent (DAKO; Carpinteria, CA) (for HAI-1) (11), by the Ventana Discovery automated staining system with a biotin-streptavidin system DAB Map kit and Amplification kit (Ventana Medical System Inc., Tucson, AZ, USA) (for PAR-2) or Vectastain ABC kit (Vector Laboratories, Burlingame, CA, USA) (for matriptase). Negative controls consisted of omission of the primary antibody. For the assessment of PAR-2 immunoreactivity in peritumoral fibroblasts, the immunostained sections were evaluated by two independent observers in a blinded fashion. Scoring was performed as follows: fibroblast PAR-2 (fPAR2) low, negative or positive in <30% of fibroblasts in the invasion front; fPAR2 high, positive in ≥30% of fibroblasts in the invasion front of OSCC. The HAI-1 immunoreactivity with special emphasis on its membranous localization was scored and reduction of the immunoreactivity in the invasion front (i.e., HAI-1 reduction level) was calculated as described previously (18). For matriptase, intensity of the immunoreactivity in OSCC was compared to that of normal oral stratified squamous epithelium in the same section, and the immunoreactivity comparable with or stronger than that of matriptase-positive normal keratinocytes was judged as positive.

Double immunofluorescence staining of PAR-2 and SMA on a single formalin-fixed paraffin embedded tissue section was performed with Opal™ 3-Plex kit (PerkinElmer Japan) according to the manufacturer's instruction. Briefly, the secondary antibody for anti-PAR-2 (SAM11) or anti-SMA was labeled with cyanine 3 (red) or fluorescein (green), followed by nuclear staining with 2-(4-amidinophenyl)-1H-indole-6-carboxamide (DAPI; blue).

Statistical analysis

Fisher's exact test and χ^2 test was used for assessment of the relationship between variables. Comparison between two groups was performed with the Mann-Whitney U test. OS and DFS were estimated using the Kaplan-Meier method where groups were compared using the log-rank test. Cox proportional hazards regression models were used to calculate the hazard ratios (HRs) and 95% confidence intervals (CIs). Patients were censored at the date of the last contact or dying of causes other than OSCC. The multivariable Cox proportional hazards regression analysis model was used to detect independent prognostic factors. Statistical significance was assumed for $p < 0.05$. Data were analyzed by StatView 5.0 (SAS Institute, Cary, NC, USA). Significance was set at $p < 0.05$.

Results

SFCM from HAI-1 knock-down SAS (HAI-1^{Low}) enhances the migration of human fibroblasts

Initially, we analyzed the effect of SFCM from parental SAS cells (HAI-1^{Cont}),

HAI-1 knock-down SAS (HAI-1^{Low}) or HAI-1^{Low} cells with engineered overexpression of HAI-1 (HAI-1^{High}) (Figure 1A) on migration and proliferation of three human fibroblast cell lines, NB1RGB, MRC5, and KD. All cell lines showed enhanced migration in response to HAI-1^{Cont} SFCM. Notably, SFCM from SAS HAI-1^{Low} cells showed an additive effect on SFCM-induced migration with NB1RGB and MRC5 cells (Figure 1B). This additive effect was completely abolished by engineered overexpression of HAI-1 in HAI-1^{Low} cells (i.e., SFCM from HAI-1^{High} cells, Figure 1B). Whereas proliferation of all fibroblast lines was modestly stimulated by HAI-1^{Cont} SFCM, neither silencing nor overexpression of HAI-1 in SAS affected the growth rate of the fibroblasts (Figure 1C).

HAI-1 silencing on SAS enhances the migration of fibroblasts by deregulating matriptase activity

HAI-1 is an efficient inhibitor of TTSP, particularly matriptase. Importantly, matriptase is an effective activator of PAR-2 (21, 25, 26) and activated fibroblasts express PAR-2 (27-31). Therefore, we hypothesized that enhanced pericellular matriptase activity due to insufficient HAI-1 may result in the activation of fibroblast PAR-2. Indeed, we previously reported that trypsin-like protease activity was increased in SFCM from HAI-1 knockdown SAS cells compared to those from parental SAS cells and, matriptase was responsible for the increased trypsin-like activity in SFCM from HAI-1 knockdown SAS using matriptase siRNA (i.e., mat siRNA #2) (18). In this study, we confirmed the above results using another matriptase siRNA (mat siRNA #1) (Figure 2A, B). The increased active matriptase in HAI-1^{Low} SFCM was also confirmed by immunoblot analysis using anti-active matriptase mAb (Supplemental Figure 1).

Then, the effects of both siRNAs (mat siRNA #1 and #2) on SFCM-induced migration of fibroblasts were examined. We found that silencing of matriptase in SAS cells alleviated the migration-inducing activity of HAI-1^{Low} SFCM, but not that of SFCM from HAI-1^{Cont} or HAI-1^{High} cells in both NB1RGB and MRC5 fibroblasts (Figure 2C).

Deregulated matriptase activity released from HAI-1^{Low} SAS enhances fibroblast migration by transactivation of fibroblast PAR-2

To test the hypothesis that the matriptase/PAR-2 pathway was involved in the enhancement of migration by HAI-1 insufficiency, we analyzed the expression of PAR-2 in the fibroblast cell lines. Of note, while all three fibroblast lines expressed only trace levels of PAR-2 mRNA and protein, the addition of SAS SFCMs induced its expression in NB1RGB and MRC5 cells, but not in KD cells (Figure 3A, B). Then, we analyzed the effect of a PAR-2 antagonist peptide (FSLRLRY-NH₂) on the migration of fibroblasts induced by SAS SFCMs. As shown in Figure 3C, the PAR-2 antagonist abolished the enhancement of fibroblast migration induced by the loss of HAI-1. We also performed migration experiments using recombinant active matriptase in the absence or presence of PAR-2 antagonist. The treatment of NB1RGB cells with matriptase (5 nM in serum-free medium) induced cellular migration, which was inhibited, at least partly, by PAR-2 antagonist (Figure 3D).

Next, we further characterized the migration response to SFCM from HAI-1^{Low} to confirm the stimulating role of fibroblast PAR-2. Toward that end, we analyzed the effects of SAS SFCMs on fibroblasts from wild-type (*F2r11*^{+/+}) or PAR-2-deficient (*F2r11*^{-/-}) mice. Rather unexpectedly, dermal fibroblasts of *F2r11*^{+/+} mice expressed a substantial level of PAR-2 even in the absence of SFCM treatment (Figure 4A). To

exclude a possibility of contamination of macrophages that express PAR-2 abundantly (36), we analyzed the expression of F4/80, a marker for murine macrophages, by RT-PCR. The cells were negative for F4/80 and showed spindle fibroblastic morphology (data not shown) so that the contamination of macrophages was unlikely. Similar to human fibroblast cell lines, both *F2r11*^{+/+} and *F2r11*^{-/-} murine fibroblasts showed migration towards SFCM of SAS cells, and *F2r11*^{+/+} fibroblasts showed enhanced migration in response to HAI-1^{Low} SFCM compared to HAI-1^{Cont} or HAI-1^{High} SFCM (Figure 4B). In contrast, the migratory response of *F2r11*^{-/-} fibroblasts was not altered by the silencing of HAI-1 in SAS (Figure 4B), indicating that fibroblast PAR-2 was responsible for the enhanced migration of fibroblasts treated with HAI-1^{Low} SFCM.

PAR-2 expression by CAFs in OSCC tissues and its prognostic impact

Finally, we examined whether CAFs in human OSCC tissues expressed PAR-2. In 95 cases of surgically resected invasive OSCC, increased PAR-2-positive peritumoral fibroblasts (i.e., fPAR2 high) was observed in 33 cases (35%) (Figure 5A-D, Supplemental Figure 2). On the other hand, in most cases, cancer cells expressed PAR-2 in varying degrees. The PAR-2-positive peritumoral fibroblasts were mostly SMA-positive (Figure 5C), which was also confirmed by a double immunofluorescence study (Figure 5D). The increased frequency of PAR-2-positive CAFs was correlated with the infiltrative morphology of the invasion front (Table 1) and likely related to OSCC cells' decreased expression of cell surface HAI-1 (Figure 5E). Among the clinicopathologic parameters examined, higher clinical disease stage, the presence of lymph node metastasis at surgery, and the absence of adjuvant therapy were correlated with poorer OS in this study cohort (Supplemental Table 2). Regarding DFS, higher

clinical disease stage, the presence of lymph node metastasis at surgery, invasive histology (i.e., Bryne invasion pattern 3 or 4), and an increased frequency of PAR-2-positive CAFs was correlated with a shorter DFS (Supplemental Table 2). A Kaplan-Meier survival analysis and a log-rank test also revealed that an increased frequency of PAR-2-positive CAFs (fPAR2 high: positive in $\geq 30\%$ of CAFs) was associated with a shorter DFS ($p = 0.0011$) (Figure 5F). When the cut-off value was set at 50% for fPAR2 high, the difference was still significant ($p = 0.0027$). To compare all prognostic factors directly in terms of their effects on patient DFS, we carried out a multivariate analysis using parameters that showed a statistically significant effect in the univariate analysis. Notably, the increased frequency of PAR-2-positive CAFs was an independent prognostic factor for DFS (HR, 2.642; 95% CI, 1.185–5.889; $p = 0.0175$) after resection of OSCC (Supplemental Table 3). We also performed immunohistochemistry for matriptase in 47 cases of OSCC and found that matriptase was positive in more than 50% of the tumor cells in most OSCC (81%, 38/47), though the intensity was varied in the tumor cells.

DISCUSSION

There is accumulating evidence that CAFs play important roles in the progression of solid cancers, including OSCC (3, 37). Many factors, such as PDGF, TGF β , bFGF, interleukin-1 and -6, tumor cell-derived exosomes and hypoxia have been reported to promote the recruitment of CAFs (38). Using OSCC as a model, this study shows that deregulated pericellular matriptase activity also contributes to the recruitment of CAF by paracrine activation of fibroblast PAR-2. Insufficient HAI-1 in OSCC cells resulted

in increased extracellular matriptase activity and activated PAR-2 expression on reactive fibroblasts, leading to enhanced migration of the fibroblasts. On the other hand, this study also confirmed that the mechanism of CAF recruitment is complex and that matriptase is one of several pro-migratory factors released by cancer cells. Nonetheless, the present clinicopathological analysis indicates that the increased frequency of PAR-2-positive CAFs at the invasion front of OSCC tissue predicts a shorter DFS of the patient after surgical resection. It should be noted that the PAR-2 immunoreactivity was observed predominantly in the cytoplasm as reported previously (31), and it is currently uncertain whether this immunoreactivity pattern represented the increased endocytosis after activation or the increased production of PAR-2.

Matriptase is known to initiate protease cascades and signaling, such as urokinase activation and HGF signaling, which are involved in cancer promotion and tumor progression (10, 23, 39). A recent report also revealed that the activation of keratinocyte PAR-2 by dysregulated matriptase is also participating in the development of squamous cell carcinoma (26). The present study may provide another possible mechanism for the matriptase-induced tumor progression, in which activation of fibroblast PAR-2 by matriptase plays a role. Matriptase is expressed in various epithelial tissues as an inactive zymogen, and its activity is tightly regulated (10, 23). Once activated on the cell surface, it is quickly inhibited by its cognate inhibitor HAI-1 (23, 32). Notably, HAI-1 was also required for the cell surface localization of matriptase (23), and in cancer cells, insufficient HAI-1 function resulted in markedly increased shedding of activated matriptase into the extracellular spaces (18, 19, 23, 40).

Enhanced matriptase immunoreactivity in OSCC and decreased cell surface HAI-1 in the invasive OSCC cells have been reported (18, 41). A preliminary

immunohistochemical analysis in this study also showed the expression of cellular matriptase in most OSCC cases, though we could not detect a statistically significant relationship between matriptase immunoreactivity and fPAR2 score (data not shown). However, as the immunohistochemical study detected total cellular matriptase that might be largely a zymogen form, it remains to be determined whether matriptase activity is in fact increased in the CAF-positive OSCC microenvironment *in vivo*. Future analysis probing the active matriptase in tissue section would be required to analyze the relationship between dysregulated matriptase and CAF recruitment.

The role of PAR-2 in cancer has been considered mostly in the tumor cells themselves (6, 39, 42-44). Although PAR-2 expression has also been observed in proliferating SMA-positive fibroblasts surrounding the carcinoma cells (31), experiments performed in PAR-2 deficient mice (*F2r11*^{-/-}) so far do not provide a clear picture of the role of PAR-2 signaling in the shaping of the tumor microenvironment. *F2r11*^{-/-} mice showed decreased tumor growth and metastasis in a spontaneous polyoma middle T breast cancer model (45), but it is unclear whether PAR-2 exerted its function in the tumor cells or the stroma in this model. When injected subcutaneously, *F2r11*^{+/+} B16 melanoma cells showed enhanced growth but less frequent pulmonary metastasis in *F2r11*^{-/-} relative to *F2r11*^{+/+} hosts, suggesting that host PAR-2 may suppress tumor growth while promoting dissemination (46). When injected intravenously, *F2r11*^{+/+} B16 melanoma cells formed lung metastases with no difference in frequency or size between *F2r11*^{-/-} and *F2r11*^{+/+} hosts (47). In a murine pancreatic cancer model, ablation of PAR-2 from the stromal compartment inhibited primary tumor growth but enhanced lymphangiogenesis and lymph node metastasis (48). Therefore, the role of stromal PAR-2 in cancer progression may depend on the primary tumor type, the model of

metastatic induction and the pericellular microenvironment. The current study revealed that a subset of OSCC cases showed PAR-2-positive CAFs in the tumor microenvironment, and the increased number of PAR-2-positive CAFs correlated with a higher histological grade of the invasion front and shorter DFS of the patient. Therefore, in OSCC, PAR-2 may help shape the microenvironment in favor of tumor progression by contributing to CAF recruitment.

On the other hand, OSCC cells themselves frequently expressed PAR-2, which has been reported to stimulate their proliferation and invasion (43). Trypsin-like serine proteases other than matriptase present in cancer tissues may also contribute to PAR-2 activation, and the *in vitro* analysis in this study cannot exclude the possibility that a trypsin-like protease activated by matriptase activated fibroblast PAR-2. A recent study reported that kallikrein-5 (KLK5) is involved in the activation of PAR-2 in OSCC and suppresses inflammation-associated tumor suppressor microRNAs via PAR-2-mediated NF- κ B signaling (44). KLK5 is also sensitive to HAI-1 (49), and lympho-epithelial Kazal-type inhibitor, the physiological inhibitor of KLK5 in keratinocytes, is downregulated in OSCC (50). Thus, when matriptase and KLK5 activities are deregulated in the OSCC microenvironment, a pericellular protease/PAR-2 axis may contribute to the invasive growth of OSCC cells through direct effects on PAR-2-positive cancer cells as well as indirectly by recruitment of PAR-2-positive CAFs. Moreover, PAR-2 activation on CAFs may provoke further mutual interactions between CAFs and adjacent OSCC cells through induced secretion of cytokines and/or growth factors involved in cancer progression, which would be a matter for future study.

In summary, this study suggests that deregulated pericellular matriptase activity

in OSCC may transactivate PAR-2 on fibroblasts in the surrounding tissue and thus promote their recruitment to the perimeter of the tumor, contributing to a microenvironment that favors tumor growth. Further studies will be required to obtain a better understanding of the matriptase/PAR-2 axis in OSCC pathology and to address whether this axis may serve as a therapeutic target for the control of OSCC progression.

Financial support:

This work was supported by a Grant-in-Aid for Scientific Research no. 24390099 and 16H05175 (H. Kataoka) from the Ministry of Education, Science, Sports and Culture, Japan, and a Grant for Clinical Research from Miyazaki University Hospital.

Disclosure statement:

Michael D. Johnson is inventor on US patent #7,355,015 (Title: Matriptase, a serine protease and its applications). Chen-Yong Lin is an inventor on US patents #6,077,938 (Title: Monoclonal antibody to an 80-kDa protease), #6,677,377 (Title: Structure based discovery of inhibitors of matriptase for the cancer diagnosis and therapy by detection and inhibition of matriptase activity), and #7,355,015 (Title: Matriptase, a serine protease and its applications).

Acknowledgements:

The authors are grateful to Ms. J. Kurogi, Ms. Y. Torisu and Mr. T Kaieda for their skillful technical assistance.

References

1. Jemal, A., Bray, F., Center, M. M., Ferlay, J., Ward, E., & Forman, D. Global cancer statistics. *CA: Cancer J Clin* 2011;61,69-90.
2. Warnakulasuriya, S. Living with oral cancer: epidemiology with particular reference to prevalence and life-style changes that influence survival. *Oral Oncology* 2010;46,407-10.
3. Hanahan D, Coussens LM. Accessories to the crime: functions of cells recruited to the tumor microenvironment. *Cancer Cell* 2012;21:309-22.
4. Kataoka, H., Miyata, S., Uchinokura, S., & Itoh, H. Roles of hepatocyte growth factor (HGF) activator and HGF activator inhibitor in the pericellular activation of HGF/scatter factor. *Cancer Metast Rev* 2003;22,223-36.
5. Coughlin, S. R. Thrombin signaling and protease-activated receptors. *Nature* 2000;407:258-64.
6. Wojtukiewicz MZ, Hempel D, Sierko E, Tucker SC, Honn K V. Protease-activated receptors (PARs)--biology and role in cancer invasion and metastasis. *Cancer Metastasis Rev* 2015;34:775-96.
7. Kataoka H, Kawaguchi M. Hepatocyte growth factor activator (HGFA): pathophysiological functions *in vivo*. *FEBS J* 2010;277:2230-7.
8. Shimomura T, Denda K, Kitamura A, Kawaguchi T, Kito M, Kondo J, Kagaya S, Qin L, Takata H, Miyazawa K, Kitamura N. Hepatocyte growth factor activator inhibitor, a novel Kunitz-type serine protease inhibitor. *J Biol Chem* 1997;272:6370-6.
9. Kawaguchi T, Qin L, Shimomura T, Kondo J, Matsumoto K, Denda K, Kitamura N. Purification and cloning of hepatocyte growth factor activator inhibitor type 2, a

- Kunitz-type serine protease inhibitor. *J Biol Chem* 1997;272:27558-64.
10. Antalis TM, Buzza MS, Hodge KM, Hooper JD, Netzel-Arnett S. The cutting edge: membrane-anchored serine protease activities in the pericellular microenvironment. *Biochem J* 2010;428:325-46.
 11. Kataoka H, Suganuma T, Shimomura T, Itoh H, Kitamura N, Nabeshima K, Koono M. Distribution of hepatocyte growth factor activator inhibitor type 1 (HAI-1) in human tissues. Cellular surface localization of HAI-1 in simple columnar epithelium and its modulated expression in injured and regenerative tissues. *J Histochem Cytochem* 1999;47:673-82.
 12. Kataoka H, Meng JY, Itoh H, Hamasuna R, Shimomura T, Suganuma T, Koono M. Localization of hepatocyte growth factor activator inhibitor type 1 in Langhans' cells of human placenta. *Histochem Cell Biol* 2000;114:469-75.
 13. Tanaka H, Nagaike K, Takeda N, Itoh H, Kohama K, Fukushima T, Miyata S, Uchiyama S, Uchinokura S, Shimomura T, Miyazawa K, Kitamura N, et al. Hepatocyte growth factor activator inhibitor type 1 (HAI-1) is required for branching morphogenesis in the chorioallantoic placenta. *Mol Cell Biol* 2005;25:5687-98.
 14. Li W, Wang B-E, Moran P, Lipari T, Ganesan R, Corpuz R, Ludlam MJC, Gogineni A, Koeppen H, Bunting S, Gao W-Q, Kirchhofer D. Pegylated Kunitz domain inhibitor suppresses hepsin-mediated invasive tumor growth and metastasis. *Cancer Res* 2009;69:8395-402.
 15. Kato M, Hashimoto T, Kataoka H, Shimomura T, Kitamura N: Hepatocyte growth factor activator inhibitor type 1 inhibits protease activity and proteolytic activation of human airway trypsin-like protease. *J Biochem* 2012;151:179-87.

16. Hashimoto T, Kato M, Shimomura T, Kitamura N. TMPRSS13, a type II transmembrane serine protease, is inhibited by hepatocyte growth factor activator inhibitor type 1 and activates pro-hepatocyte growth factor. *FEBS J* 2010;277:4888-900.
17. Fan B, Wu TD, Li W, Kirchhofer D. Identification of hepatocyte growth factor activator inhibitor-1B as a potential physiological inhibitor of prostasin. *J Biol Chem* 2005;280:34513-20.
18. Baba T, Kawaguchi M, Fukushima T, Sato Y, Orikawa H, Yorita K, Tanaka H, Lin C-Y, Sakoda S, Kataoka H. Loss of membrane-bound serine protease inhibitor HAI-1 induces oral squamous cell carcinoma cells' invasiveness. *J Pathol* 2012;228:181-92.
19. Kohama K, Kawaguchi M, Fukushima T, Lin C-Y, Kataoka H. Regulation of pericellular proteolysis by hepatocyte growth factor activator inhibitor type 1 (HAI-1) in trophoblast cells. *Hum Cell* 2012;25:100-10.
20. Xu H, Xu, Z, Tseng I-C, Chou F-P, Chen Y-W, Wang J-K, Johnson M, Kataoka H, C-Y Lin. Mechanisms for the control of matriptase activity in the absence of sufficient HAI-1. *Am J Physiol-Cell Physiol* 2012;302:C453-62.
21. Kawaguchi M, Kanemaru A, Sawaguchi A, Yamamoto K, Baba T, Lin C-Y, Johnson MD, Fukushima T, Kataoka H: Hepatocyte growth factor activator inhibitor type 1 maintains the assembly of keratin into desmosomes in keratinocytes by regulating protease-activated receptor 2-dependent p38 signaling. *Am J Pathol* 2015;185:1610-23.
22. List K, Szabo R, Molinolo A, Sriuranpong V, Redeye V, Murdock T, Burke B, Nielsen BS, Gutkind JS, Bugge TH. Deregulated matriptase causes ras-independent

multistage carcinogenesis and promotes ras-mediated malignant transformation.

Genes Dev 2005;19:1934-50.

23. Miller GS, List K. The matriptase-prostasin proteolytic cascade in epithelial development and pathology. *Cell Tissue Res* 2013;351:245-53.
24. Ustach C V, Huang W, Conley-LaComb MK, Lin C-Y, Che M, Abrams J, Kim H-RC. A novel signaling axis of matriptase/PDGF-D/ β -PDGFR in human prostate cancer. *Cancer Res* 2010;70:9631-40.
25. Camerer E, Barker A, Duong DN, Ganesan R, Kataoka H, Cornelissen I, Darragh MR, Hussain A, Zheng Y-W, Srinivasan Y, Brown C, Xu S-M, et al. Local protease signaling contributes to neural tube closure in the mouse embryo. *Dev Cell* 2010;18:25-38.
26. Sales KU, Friid S, Konkel JE, Godiksen S, Hatakeyama M, Hansen KK, Rogatto SR, Szabo R, Vogel LK, Chen W, Gutkind JS, Bugge TH. Non-hematopoietic PAR-2 is essential for matriptase-driven pre-malignant progression and potentiation of ras-mediated squamous cell carcinogenesis. *Oncogene* 2015;34:346-56.
27. Gruber BL, Marchese MJ, Santiago-Schwarz F, Martin CA, Zhang J, Kew RR: Protease-activated receptor-2 (PAR-2) expression in human fibroblasts is regulated by growth factors and extracellular matrix. *J Invest Dermatol* 2004;123:832-9.
28. Abe K, Aslam A, Walls AF, Sato T, Inoue H: Up-regulation of protease-activated receptor-2 by bFGF in cultured human synovial fibroblasts. *Life Sci* 2006;79:898-904.
29. Xue M, Chan Y-KA, Shen K, Dervish S, March L, Sambrook PN, Jackson CJ: Protease-activated receptor 2, rather than protease-activated receptor 1, contributes to the aggressive properties of synovial fibroblasts in rheumatoid arthritis. *Arthritis*

Rheum 2012;64:88-98.

30. Wygrecka M, Dahal BK, Kosanovic D, Petersen F, Taborski B, von Gerlach S, Didiasova M, Zakrzewicz D, Preissner KT, Schermuly RT, Markart P: Mast cells and fibroblasts work in concert to aggravate pulmonary fibrosis: role of transmembrane SCF and the PAR-2/PKC- α /Raf-1/p44/42 signaling pathway. *Am J Pathol* 2013;182:2094-108.
31. D'Andrea MR, Derian CK, Santulli RJ, Andrade-Gordon P. Differential expression of protease-activated receptors-1 and-2 in stromal fibroblasts of normal, benign, and malignant human tissues. *Am J Pathol* 2001;158:2031-41
32. Chen YW, Wang JK, Chou FP, Chen CY, Rorke EA, Chen LM, Chai KX, Eckert RL, Johnson MD, Lin CY. Regulation of the matriptase-prostasin cell surface proteolytic cascade by hepatocyte growth factor activator inhibitor-1 during epidermal differentiation. *J Biol Chem* 2010;285:31755-62.
33. Imaging a functional tumorigenic biomarker in the transformed epithelium. LeBeau AM, Lee M, Murphy ST, Hann BC, Warren RS, Delos Santos R, Kurhanewicz, J, Hanash SM, VanBrocklin HF, Craik CS. *Proc Na Acad Sci USA* 2013;110:93-8.
34. Lindner JR, Kahn ML, Coughlin SR, Sambrano GR, Schauble E, Bernstein D, Foy D, Hafezi-Moghadam A, Ley K. Delayed onset of inflammation in protease-activated receptor-2-deficient mice. *J Immunol* 2000;165:6504-10
35. Bryne M, Jenssen N, Boysen M. Histological grading in the deep invasive front of T1 and T2 glottic squamous cell carcinomas has high prognostic value. *Virchows Archiv* 1995;427:277-81.
36. Lohman R-J, Cotterell AJ, Barry GD, Liu L, Suen JY, Vesey DA, Fairlie DP. An antagonist of human protease activated receptor-2 attenuates PAR2 signaling,

macrophage activation, mast cell degranulation, and collagen-induced arthritis in rats. *FASEB J* 2012;26:2877-87.

37. Bello IO, Vered M, Dayan D, Dobriyan A, Yahalom R, Alanen K, Nieminen P, Kantola S, Läärä E, Salo T. Cancer-associated fibroblasts, a parameter of the tumor microenvironment, overcomes carcinoma-associated parameters in the prognosis of patients with mobile tongue cancer. *Oral Oncol.* 2011;47:33-8.
38. Ohlund D, Elyada E, Tuveson D: Fibroblast heterogeneity in the cancer wound. *J Exp Med* 2014;211:1503-23.
39. Szabo R, Rasmussen AL, Moyer AB, Kosa P, Schafer JM, Molinolo AA, Gutkind JS, Bugge TH. c-Met-induced epithelial carcinogenesis is initiated by the serine protease matriptase. *Oncogene* 2011;30:2003–16.
40. Ye J, Kawaguchi M, Haruyama Y, Kanemaru A, Fukushima T, Yamamoto K, Lin C-Y, Kataoka H: Loss of hepatocyte growth factor activator inhibitor type 1 participates in metastatic spreading of human pancreatic cancer cells in a mouse orthotopic transplantation model. *Cancer Sci* 2014;105:44-51.
41. Cheng MF, Huang MS, Lin CS, Lin LH, Lee HS, Jiang JC, Hsia KT. Expression of matriptase correlates with tumour progression and clinical prognosis in oral squamous cell carcinoma. *Histopathol* 2014;65:24-34.
42. Chang L-H, Pan S-L, Lai C-Y, Tsai A-C, Teng C-M: Activated PAR-2 regulates pancreatic cancer progression through ILK/HIF- α -induced TGF- α expression and MEK/VEGF-A-mediated angiogenesis. *Am J Pathol* 2013;183:566-75.
43. Kamal Al-Eryani, Jun Cheng, Tatsuya Abé, Satoshi Maruyama, Manabu Yamazaki, Hamzah Babkair, Ahmed Essa, Takashi Saku. Protease-activated receptor 2 modulates proliferation and invasion of oral squamous cell carcinoma cells. *Hum*

Pathol 2015;46:991-9.

44. Johnson JJ, Miller DL, Jiang R, Liu Y, Shi Z, Tarwater L, Williams R, Balsara R, Sauter ER, Stack MS. Protease activated receptor-2 (PAR-2)-mediated Nf- κ B activation suppresses inflammation-associated tumor suppressor microRNAs in oral squamous cell carcinoma. *J Biol Chem* 2016;291:6936-45
45. Versteeg HH1, Schaffner F, Kerver M, Ellies LG, Andrade-Gordon P, Mueller BM, Ruf W. Protease-activated receptor (PAR) 2, but not PAR1, signaling promotes the development of mammary adenocarcinoma in polyoma middle T mice. *Cancer Res* 2008;68:7219-27.
46. Olejar T, Vetvicka D, Zadinova M, Pouckova P, Kukal J, Jezek P, Matej R. Dual role of host Par2 in a murine model of spontaneous metastatic B16 melanoma. *Anticancer Res* 2014;34:3511-5.
47. Camerer E, Qazi AA, Duong DN, Cornelissen I, Advincula R, Coughlin SR. Platelets, protease-activated receptors, and fibrinogen in hematogenous metastasis. *Blood* 2004;104:397-401.
48. Shi K, Queiroz KCS, Roelofs JJTH, van Noesel CJM, Richel DJ, Spek CA: Protease-activated receptor 2 suppresses lymphangiogenesis and subsequent lymph node metastasis in a murine pancreatic cancer model. *J Pathol* 2014;234:398-409.
49. Mukai S, Fukushima T, Naka D, Tanaka H, Osada Y, Kataoka H. Activation of hepatocyte growth factor activator zymogen (pro-HGFA) by human kallikrein 1-related peptidases. *FEBS J* 2008;275:1003-17.
50. Gonzalez HE, Gujrati M, Frederick M, Henderson Y, Arumugam J, Spring PW, Mitsudo K, Kim HW, Clayman GL. Identification of 9 genes differentially expressed in head and neck squamous cell carcinoma. *Arch Otolaryngol Head Neck*

Figure Legends

Figure 1. Effects of SAS SFCM on fibroblast cell lines. (A) Immunoblot analysis for HAI-1 expression by SAS and its sublines. HAI-1^{Cont}, parent SAS; HAI-1^{Low}, stable HAI-1 knock-down SAS; mock, mock-transfected HAI-1^{Low} cells; HAI-1^{High}, HAI-1 expressing vector-transfected HAI-1^{Low} cells. (B) Effect on cellular migration. 1×10^4 fibroblasts in 100 μ L DMEM/0.1 % BSA were placed in the upper compartment and the lower compartment contained serum-free DMEM/0.1% BSA without (indicated as medium) or with SFCM equivalent to 2 μ g of total proteins (SAS SFCM). *, $p < 0.001$ compared to other groups; **, $p < 0.05$; $n = 9$. Error bar, standard deviation (SD). (C) Effect on cellular proliferation. *, $p < 0.05$ compared to other groups; $n = 3$. Error bar, SD.

Figure 2. Enhanced matriptase activity in HAI-1-deficient SAS SFCM and its role in fibroblast migration. (A) Efficiency of matriptase knock down by siRNA. Parental (HAI-1^{Cont}), HAI-1 knock-down (HAI-1^{Low}) and HAI-1 overexpressing (HAI-1^{High}) SAS cells were treated with two kinds of matriptase siRNAs; matriptase siRNA #1 (si-mat #1) and matriptase siRNA#2 (si-mat #2). Control siRNA (si-NC)-treated cells were also analyzed. Immunoblot data of total matriptase (mAb M24) of the cell extracts 3 days after siRNA transfection are shown. (B) Enhanced trypsin-like protease activity in response to HAI-1 knock down. Representative data of boc-Glu(OBzl)-Ala-Arg-AMC hydrolysis activities in SFCM indicated by RFU are

shown in the left panel. The maximum slope of the hydrolysis rate was calculated (V_{max}) and the effect of matriptase silencing on V_{max} value is shown in the right panel. Error bar, standard deviation (SD) of three independent experiments. *, $p < 0.001$. (C) Knock-down of matriptase in parental SAS and its sublines: impact on migration of NB1RGB and MRC5 fibroblast cell lines treated with SAS SFCM. Cells of different population doubling levels (PDL) indicated in the figure were used for two independent experiments of each fibroblast line. $N = 9$ in each experiment. *, $p < 0.01$.

Figure 3. Expression of PAR-2 in fibroblasts and the effect of a PAR-2 antagonist on SAS SFCM-induced fibroblast migration. (A) RT-PCR analysis for the *F2RL* gene expression by three fibroblast cell lines (NB1RGB, MRC5, KD) treated without (medium) or with three kinds of SAS SFCM. The fibroblasts were cultured on type I collagen-coated dishes. (B) Immunoblot analysis of PAR-2 in NB1RGB cells. NB1RGB cells were cultured on plastic or type I collagen-coated dish without (medium) or with SAS SFCM. Semiquantitation of the PAR-2 protein band normalized to corresponding caveolin protein band and mean \pm SD of three independent experiments is indicated in the right panel. (C) Effects of PAR-2 antagonist (10 μ M) on SAS SFCM-induced migration of fibroblast cell lines. *, $p < 0.05$ compared to other groups. (D) Effect of recombinant matriptase on migration of NB1RGB cells. 1×10^4 NB1RGB cells in 100 μ L DMEM/0.1 % BSA were placed in the upper compartment and the lower compartment contained serum-free DMEM/0.1% BSA without or with 5 nM of recombinant matriptase (catalytic domain). Effect of PAR-2 antagonist was also examined. *, $p < 0.0001$; $n = 10$. Error bar, SD.

Figure 4. Effects of SAS SFCMs on mouse fibroblasts derived from wild-type or PAR-2 knockout mice. (A) RT-PCR for the *F2rl1* gene in dermal fibroblasts from PAR-2 knockout (*F2rl1*^{-/-}) mouse and its littermate controls, wild-type (*F2rl1*^{+/+}) and PAR-2 heterozygous (*F2rl1*^{+/-}) mice. (B) Effects of SAS SFCM on migration of wild-type and PAR-2 knockout mouse fibroblasts. *, $p < 0.0001$ compared to other groups; **, $p < 0.01$; n = 9.

Figure 5. Expression of PAR-2 in CAFs of human OSCC tissues and its prognostic impact. (A) Representative images of hematoxylin-eosin stained section (HE) and PAR-2 immunohistochemistry of fibroblasts. This example represents fPAR2 high. *, separation artifact; bar, 50 μ m. (B) A representative image of an OSCC case with fPAR2 low. Bar, 100 μ m. (C) High magnification image of PAR-2-positive CAFs. Serial sections were stained for PAR-2 (upper panel) and SMA (lower). Arrows indicate representative examples of PAR-2/SMA double positive peritumoral fibroblasts. Bar, 50 μ m. (D) Double immunofluorescence staining for PAR-2 and SMA. PAR-2 (red)-positive CAFs are also positive for SMA (green). T, tumor cell nest. Note that OSCC cells in all images (A-D) are positive for PAR-2 in varying degrees. (E) Relationship of fibroblast PAR-2 score (fPAR2) to decreased cell surface HAI-1 immunoreactivity at the OSCC invasion front. Calculation of HAI-1 reduction level at the invasion front was performed as described previously (18). The boxes show the interquartile ranges, the whiskers the largest and smallest observed scores that are < 1.5 box lengths from the end of the box, and the median is indicated by a bold vertical line; circles represent cases with scores > 1.5 box lengths from the end of the box. *, $p < 0.05$. (F) Kaplan–Meier survival curves. Patients with fPAR2 high were compared to those

with fPAR2 low. OS and DFS after surgical resection of OSCC were analyzed. *P* value was calculated by log-rank test.

Supplemental Figure 1. Immunoblot analysis of active-form matriptase in SFCM.

Concentrated SFCM that was equivalent to protein amount of 2 μ g was subjected to immunoblot analysis using mAb A11 (33) under reducing condition.

An immunoreactive band around 25~27kDa (arrow), which likely represents an active form of matriptase (33), is increased in HAI-1Low SFCM compared to control and HAI-1High SFCM.

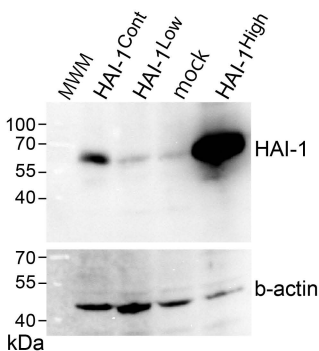
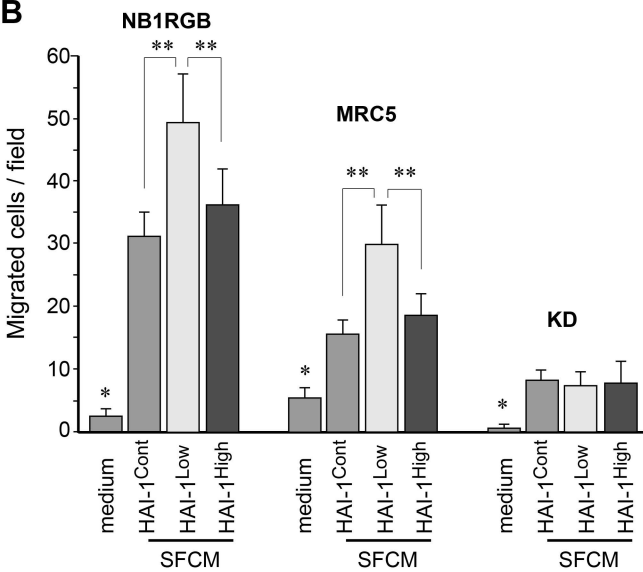
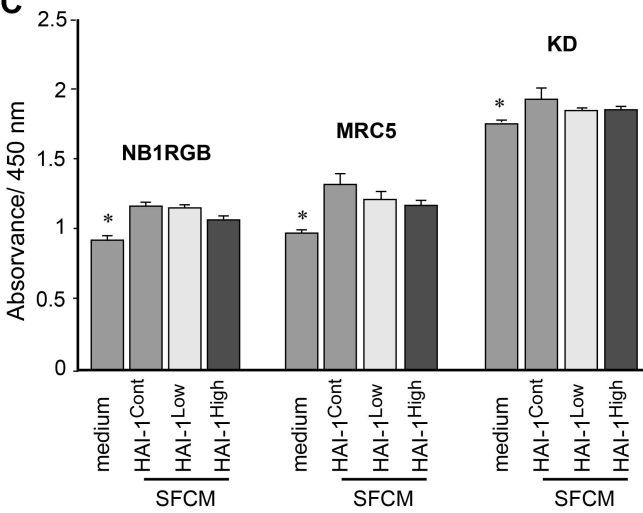
Supplemental Figure 2. Immunohistochemistry for PAR-2 and matriptase in OSCC.

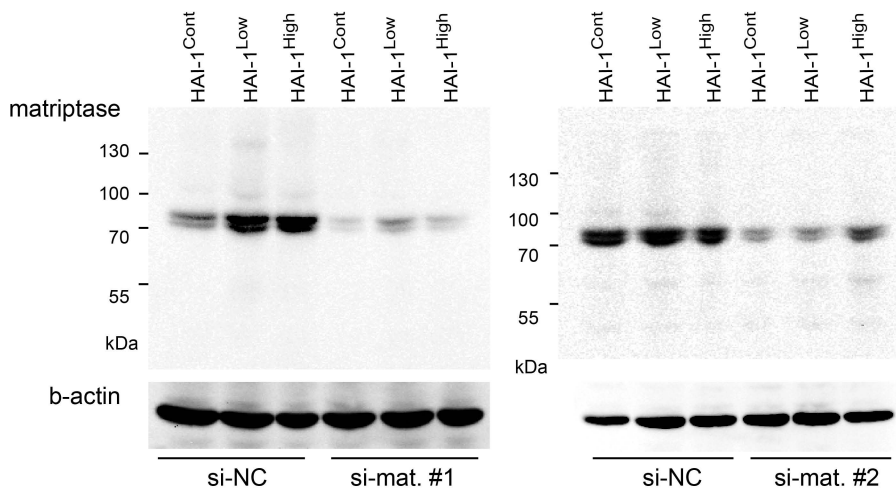
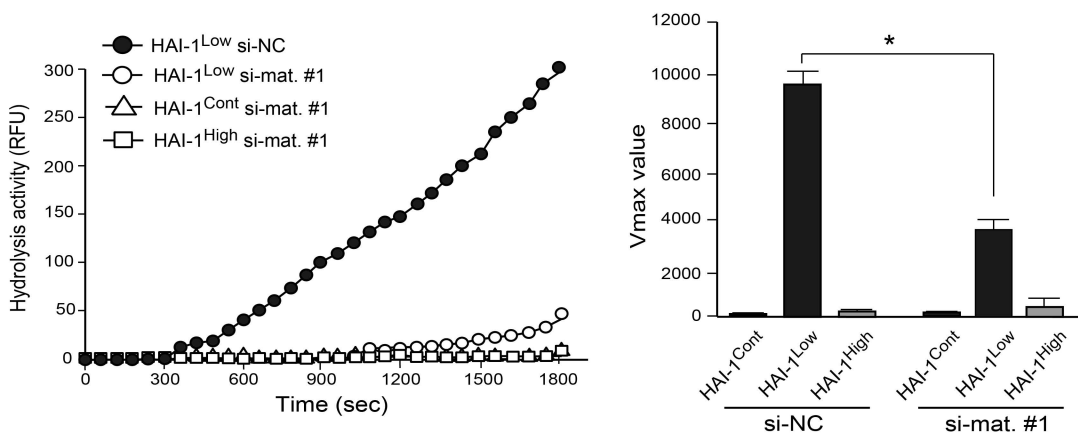
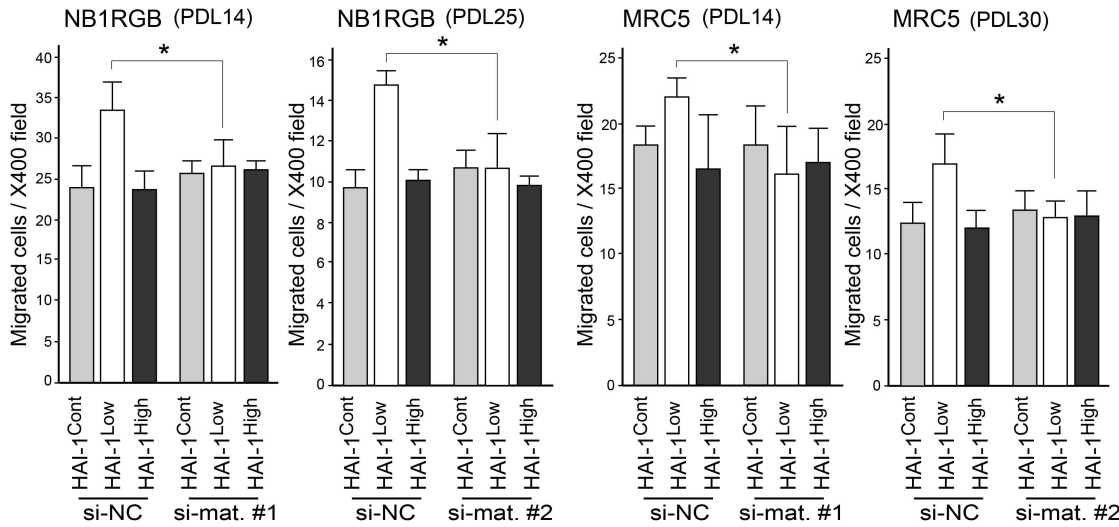
(A) PAR-2 immunohistochemistry. Representative photos of fPAR2 high, fPAR2 low and negative control (NC) are shown. Bar, 50 μ m. (B) Matriptase immunohistochemistry. Representative photos of matriptase positive OSCC (left) and negative control (NC) are shown. Bar, 50 μ m.

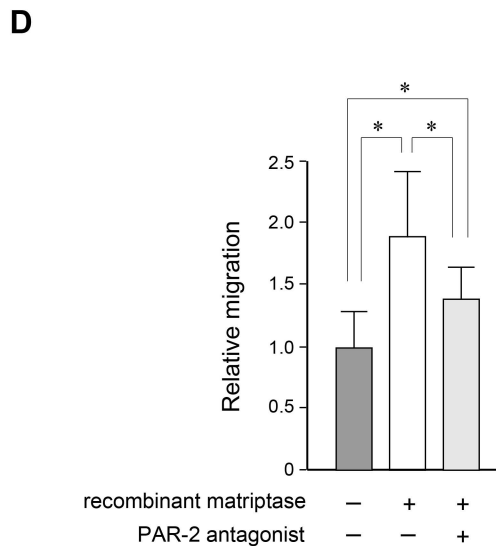
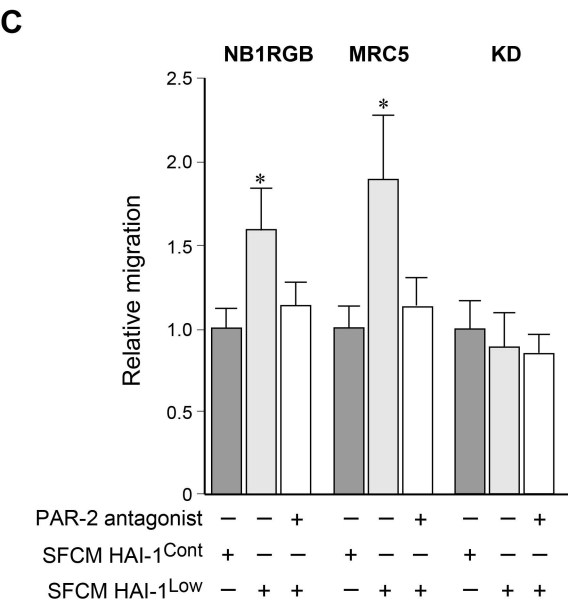
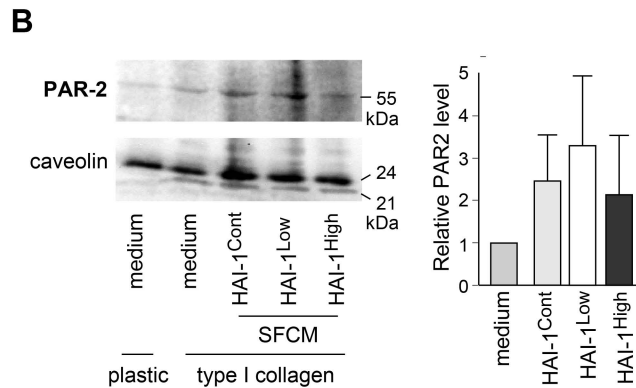
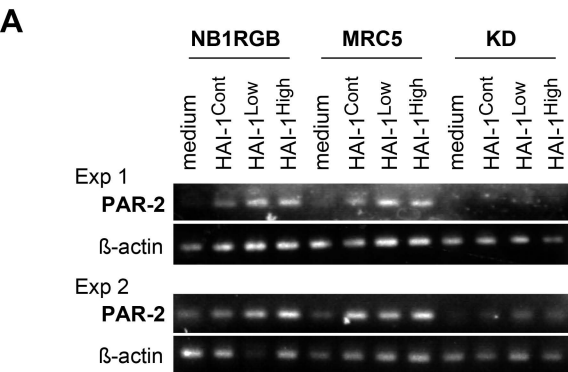
Table 1. Correlation between PAR-2 expression and clinicopathological data

Parameters		total	PAR-2-positive fibroblasts			P value*
			fPAR2 Low		fPAR2 High	
			none	< 30%	≥ 30%	
Gender	Male	59	17	13	19	0.5090
	Female	36	16	6	14	
Age	≥ 60	72	33	12	27	0.3195
	< 60	23	10	7	6	
T stage	T3 + T4	16	3	7	6	0.8001
	T1 + T2	79	40	12	27	
Lymph node metastasis at surgery	Yes	21	6	4	11	0.0556
	No	74	37	15	22	
Clinical disease stage	III + IV	31	9	9	13	0.3076
	I + II	64	34	10	20	
Adjuvant therapy	Yes	45	22	6	17	0.6614
	No	50	21	13	16	
Bryne invasion pattern	3 + 4	44	15	7	22	0.0039
	1 + 2	51	28	12	11	
Tumor histological grade	Mod. + Poor	21	11	3	7	0.8790
	Well	74	32	16	26	

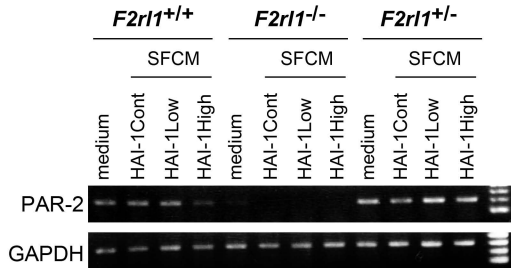
*, χ^2 test

A**B****C**

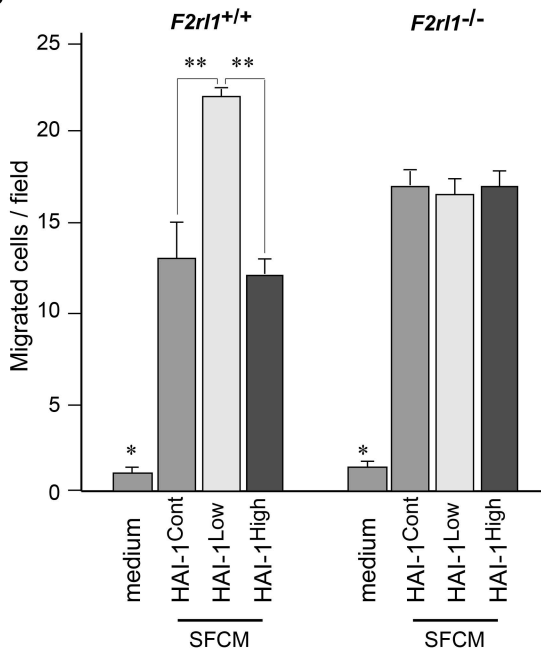
A**B****C**

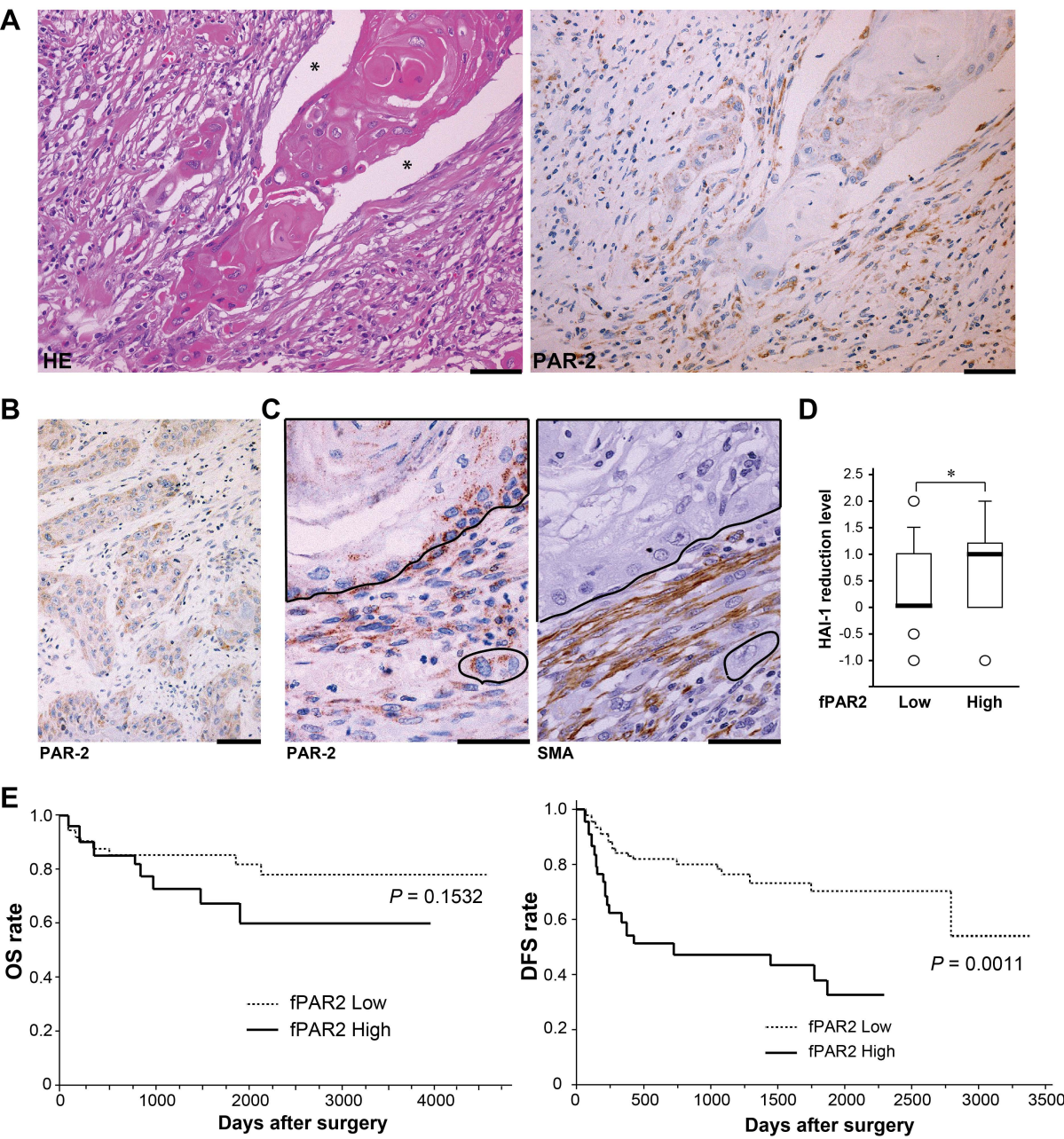


A



B





Supplemental Table 1: Baseline characteristics of OSCC cases (n = 95)

Characteristic	n (%)
Gender	
Male	59 (62.1)
Female	36 (37.9)
Age	
≥ 60	72 (75.8)
< 60	23 (24.2)
T stage	
T1	27 (28.4)
T2	52 (54.7)
T3	6 (6.3)
T4	10 (10.6)
Clinical disease stage	
I	21 (22.1)
II	43 (45.3)
III	14 (14.7)
IV	17 (17.9)
Lymph node metastasis at surgery	
No	74 (77.9)
Yes	21 (22.1)
Adjuvant therapy	
No	50 (52.6)
Yes	45 (47.4)
Bryne invasion pattern	
1	19 (20.0)
2	32 (33.7)
3	33 (34.7)
4	11 (11.6)
Tumor histological grade	
Well	74 (72.9)
Moderate	19 (20.0)
Poor	2 (2.1)

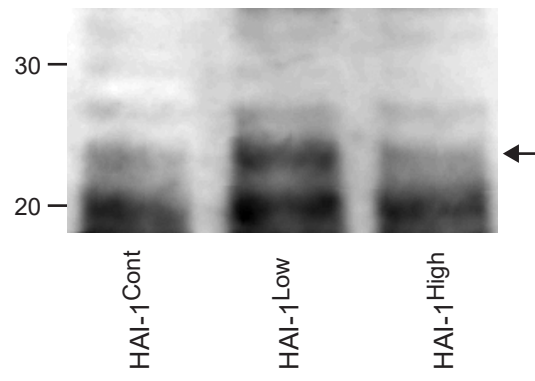
Supplemental Table 2: Univariate analysis of clinicopathological parameters for OS and DFS

Parameters	OS (n=95)			DFS (n=95)		
	HR	(95% CI)	<i>p</i> value	HR	(95% CI)	<i>p</i> value
Age (≥60 vs. <60)	2.827	0.650-12.304)	0.1660	1.251	(0.555-2.816)	0.5892
Gender (male vs. female)	1.054	(0.408-2.720)	0.9136	1.595	(0.795-3.203)	0.1888
T stage (T3/4 vs. T1/2)	1.055	(0.305-3.646)	0.9325	1.218	(0.501-2.961)	0.6639
Clinical disease stage (III/IV vs. I/II)	3.659	(1.417-9.450)	0.0074	2.135	(1.073-4.246)	0.0307
Lymph node metastasis at surgery (+ vs. -)	5.458	(2.146 - 13.880)	0.0004	2.648	(1.270-5.521)	0.0094
Adjuvant therapy (- vs. +)	2.983	(1.061-8.391)	0.0383	1.165	(0.587-2.312)	0.6614
Bryne invasion pattern (3/4 vs. 1/2)	1.951	(0.754-5.047)	0.1683	2.227	(1.103 -4.499)	0.0256
Tumor histological grade (mod./poor vs. well)	2.302	(0.892-5.942)	0.0848	1.081	(0.468-2.497)	0.8546
Fibroblast PAR-2 score (fPAR2) (high vs. low)	1.937	(0.768-4.884)	0.1614	3.035	(1.507-6.114)	0.0019

Supplemental Table 3: Multivariate analysis of clinicopathological parameters for OS and DFS

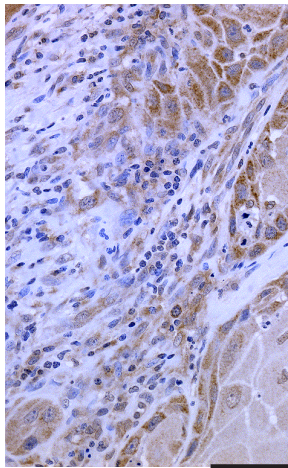
Parameters	OS (n=95)			DFS (n=95)		
	HR	(95% CI)	<i>p</i> value	HR	(95% CI)	<i>p</i> value
Clinical disease stage (III/IV vs. I/II)	0.960	(0.159-5.793)	0.9647	1.764	(0.551-5.651)	0.3393
Lymph node metastasis at surgery (+ vs. -)	6.000	(1.021-35.269)	0.0474	0.975	(0.262-3.636)	0.9705
Adjuvant therapy (- vs. +)	3.245	(1.148-9.171)	0.0264			
Bryne invasion pattern (3/4 vs. 1/2)				1.450	(0.651-3.229)	0.3633
Fibroblast PAR-2 score (fPAR2) (high vs. low)				2.642	(1.185-5.889)	0.0175

Supplemental Figure 1

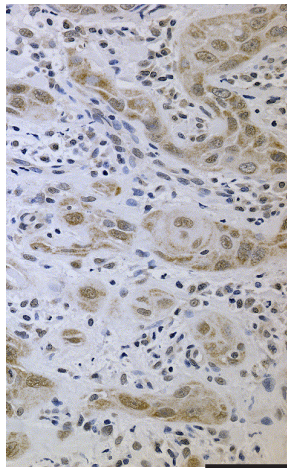


Supplemental Figure 2

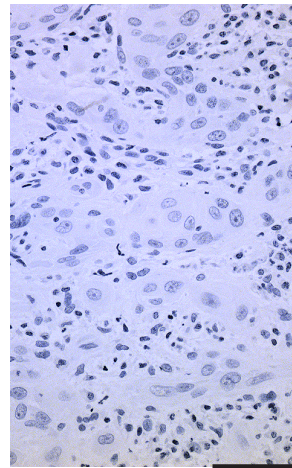
A



fPAR2 high

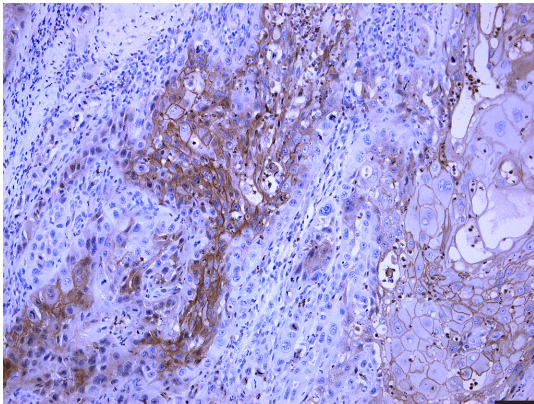


fPAR2 low

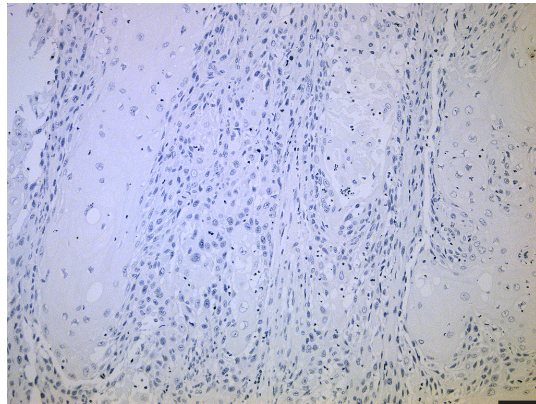


NC

B



matriptase



NC

IJC

International Journal of Cancer

Cell line confirmation form

Date: April 20, 2016

Title of manuscript: Deregulated matrilysin activity in oral squamous cell carcinoma promotes the infiltration of cancer-associated fibroblasts by paracrine activation of protease-activated receptor 2

Corresponding author name: Hiroaki Kataoka

We have used the following human cell lines in our study:

SAS (Cell Resource Center for Biomedical Research, Tohoku University: ID TKG0470) human squamous cell carcinoma of tongue
Subclones of SAS, namely SAS HAI-1Low and SAS HAI-1High
Human normal fibroblast cell line NB1RGB provided and authorized by Riken Cell Bank
Human normal fibroblast cell line MRC5 provided and authorized by Japanese Cancer Research Resources Bank
Human normal fibroblast cell line KD provided and authorized by Japan Health Science Foundation

and confirm that all DNA profiles for the aforementioned lines have been counterchecked with the DNA profile of the donor tissue (in case of a new cell line) and compared with the DNA profile of other continuous cell lines such as provided by the data bank available through www.dsmz.de/fp/cgi-bin/str.html and shown to be authentic.

Signature: 